Novel liposome-like assemblies composed of phospholipid-porphyrin conjugates with photothermal and photodynamic activities against bacterial biofilms

Paul Cressey, Louis-Gabriel Bronstein, Rayene Benmahmoudi, Véronique Rosilio, Christophe Regeard, Ali Makky

Novel liposome-like assemblies composed of phospholipid-porphyrin conjugates with photothermal and photodynamic activities against bacterial biofilms

Paul Cressey[a#], Louis-Gabriel Bronstein[a#], Rayene Benmahmoudi[a,b], Véronique Rosilio[a],

Christophe Regeard[b]* and Ali Makky[a] *

[a] Université Paris-Saclay, CNRS, Institut Galien Paris-Saclay, 92296, Châtenay-Malabry cedex, France

[b] I2BC - Institut de Biologie Intégrative de la Cellule, 91198, Gif sur Yvette cedex, France

* Corresponding authors: christophe.regeard@universite-paris-saclay.fr, ali.makky@universite-paris-saclay.fr

[#] Equally contributed

Abstract

Phospholipid-Porphyrin (PL-Por) conjugates are unique building blocks that can self assemble into liposome-like structures with improved photophysical properties compared to their monomeric counterparts. The high packing density of porphyrin moieties enables these assemblies to exhibit high photothermal conversion efficiency as well as photodynamic activity. Thus, PL-Por conjugates assemblies can be used for photodynamic therapy (PDT) and photothermal therapy (PTT) applications against resistant bacteria and biofilms. In order to tune the PD/PT properties of such nanosystems, we developed six different supramolecular assemblies composed of newly synthesized PL-Por conjugates bearing either pheophorbide-a (Ph_xLPC) or pyropheophorbide-a (Pyr_xLPC) PSs for combined PDT/PTT against planktonic bacteria and their biofilms. In this study, the influence of the chemical structure of the phospholipid backbone as well as that of the PS on the photothermal conversion efficiency, the photodynamic activity and the stability of these assemblies in biological medium were determined. Then their antimicrobial efficiency was assessed on *S. aureus* and *P. aeruginosa* planktonic cultures and biofilms. The two studied systems show almost the same photothermal effect against planktonic cultures and

biofilms of *S. aureus* and *P. aeruginosa*. However, Ph_xLPC vesicles exhibit superior photodynamic activity, making them the best combination for PTT/PDT. Such results highlight the higher potential of the photodynamic activity of PL-Por nanoassemblies compared to their photothermal conversion in combating bacterial infections.

Keywords: Phospholipid-porphyrin conjugate, photodynamic therapy, photothermal therapy, biofilm.

1. Introduction

Developing new treatments for bacterial infections is paramount to maintain human health. According to the WHO, in the absence of new treatments to combat rising antimicrobial resistance, deaths due to drug-resistant microbes will increase from ~700,000 per year to 10 million per year in ~2050 (de Kraker et al., 2016; WHO, 2019). These estimated projections may be further exacerbated by the overuse of antibiotics in hospitalized patients in many countries during the first wave of COVID-19 pandemic, despite the rare incidence of bacterial co-infections (Manesh and Varghese, 2021). Bacteria can become resistant to antibiotics through a wide range of mechanisms, including modifying the antibiotic target, *in situ* inactivation of the antibiotic, active efflux of the antibiotic, or by limiting uptake of the antibiotic (Reygaert, 2018). Another common antimicrobial resistance mechanism that bacteria can develop is based on the growth of bacteria as biofilm. Biofilms are a complex organization of single or multi-bacterial species embedded in a protective extracellular polymeric matrix (Flemming and Wingender, 2010) which is generally composed of exopolysaccharides, proteins and sometimes DNA. Such a matrix presents strong adhesion to living or inert surfaces and interfaces (Hall-Stoodley et al., 2004) and limits the accessibility of antibiotics to bacteria clustered within the biofilm.

Therefore, the development of alternative treatments that can disrupt a biofilm and dissociate the bacteria hiding within this complex structure is of great clinical importance. Some progress has been made with positive results reported for antimicrobial photodynamic therapy (aPDT) and photothermal therapy (PTT). (Aksoy et al., 2020; Qayyum and Khan, 2016) aPDT and PTT are light-based treatment modalities. While PDT relies on the combination of a light source, a photosensitizer (PS) and oxygen to produce, through photochemical reactions, reactive oxygen species (ROS) that are highly toxic for bacteria, PTT consists in the conversion of light absorbed by photothermal agents into cytotoxic heat. Both treatment modalities present promising results, however combining them in one nanoplatform could provide higher efficacy to eradicate completely of a biofilm and the bacteria within. Nevertheless, the design of such nanoplatforms usually requires the conjugation of a photosensitizer to a photothermal agent such as gold or semiconductor polymeric nanoparticles that need multiple steps of chemical functionalization, purification and characterization, jeopardizing their clinical translation (Zmerli et al., 2021a; Zmerli et al., 2021b).

Beside this strategy, the PDT/PTT combination could also be achieved using a single organic building block such as phospholipid-porphyrin conjugates (PL-Por), which are currently considered as versatile materials for the development of smart drug delivery systems based on their supramolecular assemblies. These latter exhibit attractive multifunctional activities such as PTT, PDT, photoacoustic imaging (PA) or photo-triggered release.(Carter et al., 2014; Lovell et al., 2011) Indeed, PL-Por conjugates can self-assemble into liposome-like structures, where the porphyrin moieties are tightly packed together leading to an intensive quenching of their fluorescent properties. Fluorescence quenching allows the assemblies to act as photothermal agents upon near infrared (NIR) irradiation. Then, *in situ*, the nanostructures can passively disassemble regenerating the fluorescent properties as well as the photodynamic activity of the

photosensitizer. However, despite the versatility of these compounds, there are no studies about their use and their antimicrobial efficiency against planktonic bacteria and/or their biofilms. In addition, there are no previous reports on the impact of the photodynamic/photothermal balance offered by the same nanoplatforms on their antimicrobial activities.

Herein, we developed different liposome-like assemblies composed of newly synthesized phospholipid-porphyrin conjugates for bimodal PTT/PDT of planktonic bacteria and their biofilms. The conjugates exhibit different alkyl chain lengths in sn2 position and are linked to either pheophorbide-a (Ph_xLPC) or pyropheophorbide-a (Pyr_xLPC) (Bronstein et al., 2022a; Bronstein et al., 2022b) via amide coupling (Figure 1). In a previous work, we studied the 2D phase behavior of these conjugates at the air/water interface (Bronstein et al., 2022a). This study revealed that Pyro-a conjugates have the tendency to form well structured domains due to the higher π-π stacking compared to Pheo-a conjugates. This may have a great impact on the photophysical properties of the assemblies but also on the propensity of the conjugates to form stable structures. Indeed, these conjugates proved unable to form stable structures by themselves and could not be incorporated even at low molar ratio (10 mol %) into conventional phospholipid matrices without destabilizing their structure (Bronstein et al., 2022b). To overcome such problem, we optimized the formulation of the assemblies by mixing PL-Por conjugates with helper lipids such as cholesterol which may (i) exhibit a complementary geometrical packing parameter (Massiot et al., 2022; Massiot et al., 2019) compared to PL-Por conjugates and/or (ii) reduce the propensity of π-π stacking between the porphyrin cores leading to the formation of stable liposome-like structures (Massiot et al., 2022). This allowed the formation of stable assemblies that preserved their structure in biological media. While changing the porphyrin core controls the fluorescence quenching and the photothermal/photodynamic activities of the

conjugates assemblies, tuning the linker length can control their packing inside the supramolecular assemblies and thus their stabilities in biological media. We quantified the photothermal effect as well as the photodynamic effect of the most promising formulations. Finally, as proof of concept, the efficiency of the bimodal PTT/PDT nanosystems was evaluated *in vitro* on planktonic cultures and on biofilms of the Gram negative bacteria *Pseudomonas aeruginosa* and Gram positive bacteria *Staphylococcus aureus*.

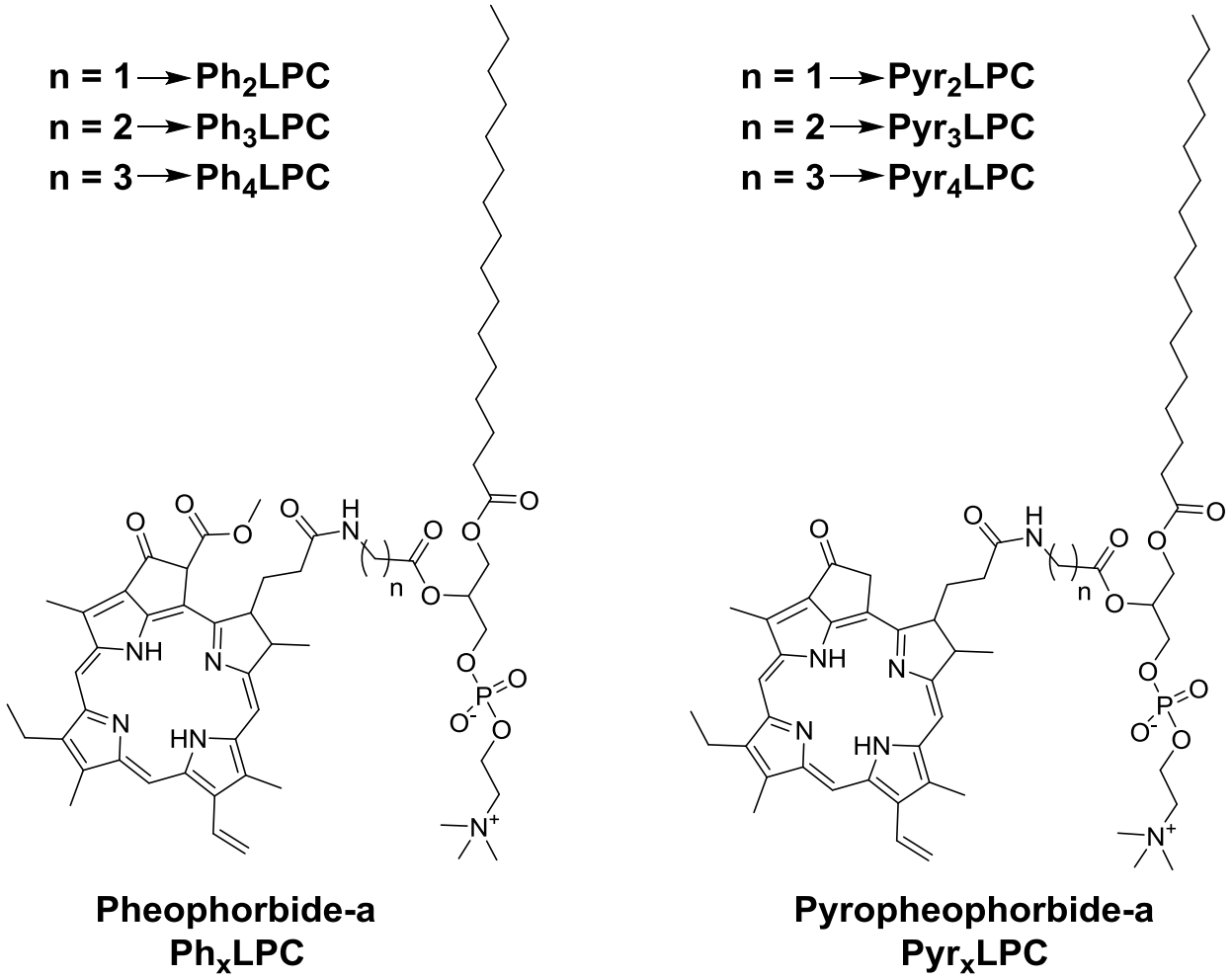

Figure 1: Structure of lipid-porphyrin conjugates Ph_xLPC and Pyr_xLPC bearing pheophorbide-a and pyropheophorbide-a chromophores, respectively.

2. Material and methods

2.1. Chemicals

Pheophorbide a (Pheo-a, ≥ 95%, mixture of diastereomers, Mw = 592.69 g/mol) and pyropheophorbide a (Pyro-a, ≥ 95%, Mw = 534.66 g/mol) was purchased from Frontier Scientific (Logan, UT). HEPES (99.5%, Mw = 238.31 g/mol), sodium chloride (NaCl, 99%, Mw = 58.44 g/mol), cholesterol (Chol, ≥99% pure, Mw = 386.65 g/mol), 9,10-anthracenediyl-bis(methylene) dimalonic acid (ABDA) and Triton^{TM} X-100 were purchased from Sigma (St. Louis, MO, USA). The phospholipids 1,2-dipalmitoyl-sn-glycero-3-phosphocholine (16:0 DPPC, 99%, Mw = 733.52 g/mol) and 1,2-distearoyl-sn-glycero-3-phosphoethanolamine-N-[amino(polyethyleneglycol)-2000] (ammonium salt) (DSPE-mPEG$_{2000}$, 99%, Mw = 2805.497 g/mol) were purchased from Avanti Polar Lipids (Alabaster, AL). Chloroform and methanol analytical-grade reagents were purchased from Carlo Erba (Val-de-Reuil, France). The ultrapure water (γ = 72.2 mN/m at 22° C) used in all experiments was produced by a Millipore Milli-Q® Direct 8 water purification System, with a resistivity of 18.2 MΩ.cm. Ph$_X$LPC and Pyr$_X$LPC were prepared as previously described(Bronstein et al., 2022a; Bronstein et al., 2022b).

2.2. Preparation and characterization of self-assembled structures or liposomes.

The self-assembled structures made of lipid-porphyrin conjugates were prepared by the thin lipid film hydration method followed by extrusion of the vesicles.(Zhang, 2017) Mixtures of cholesterol, DSPE-PEG$_{2000}$ and phospholipid-porphyrin (PL-Por) conjugate (47.5: 47.5: 5 mol%, Chol: PL-Por: DSPE-PEG$_{2000}$) were prepared in chloroform: methanol (9:1 v/v). After removing the organic solvent under vacuum at 45 °C, the resulting film was rehydrated with 1 mL of HEPES buffer, to get a final lipid concentration of 2 mM. The mixture was vortexed at 70°C for 5 min. The suspension was then extruded 21 times through a 200 nm pore-sized polycarbonate

membrane, while maintaining the temperature at 70 °C. The hydrodynamic diameter was measured by dynamic light scattering (DLS) (Nano ZS90, Malvern). All measurements were carried out at 25 °C.

2.3. Cryogenic electron transmission electron microscopy (Cryo-TEM)

The self-assembled structures made of lipid-porphyrin conjugates mixed with Chol:DSPE-PEG_{2000} (molar percentage of 47.5:47.5:5) were deposited on perforated carbon-coated, copper grid (TedPella, Inc) which was immediately plunged into a liquid ethane bath cooled with liquid nitrogen (-180 °C) and then mounted on a cryo holder(da Cunha et al., 2016). Cryo-transmission electron microscopy (Cryo-TEM) measurements were then performed using a JEOL 2200FS (JEOL USA, Inc., Peabody, MA, U.S.A.) working under an acceleration voltage of 200 kV (Institut Curie). Electron micrographs were recorded by a CCD camera (Gatan, Evry, France).

2.4. Absorption and Fluorescence Measurements

UV–visible absorption measurements were carried out on a CARY 300 Bio UV–visible spectrophotometer (Varian, USA). Fluorescence emission spectra were recorded on a Perkin-Elmer LS-50B luminescence spectrometer (MA, USA) equipped with a red sensitive photomultiplier. Excitation of porphyrins was performed at the maximum of the Soret band (415 nm) at a concentration of 4 μM of PL-Por.

Calibration curves for each conjugate were extrapolated by measuring the absorbance of PL-Por in $CHCl_3$:MeOH (9:1) over a range of concentrations (0.1 to 2 μM) at 667 nm. Their content in the assemblies was evaluated by removing 10 μL from the formulation, drying under vacuum before dissolving in $CHCl_3$:MeOH (9:1) and the absorbance compared to the calibration curves.

2.5. Assessment of the stability under physiological conditions

The stability of each formulation in physiological medium was assessed by fluorescence measurements using a Perkin-Elmer LS-50B luminescence spectrometer (MA, USA) equipped with a red sensitive photomultiplier. 10% of fetal bovine serum (FBS) (v/v) was added to each liposomal suspension at 37°C. Then the fluorescence at λ_{ex} of 415 nm of each suspension was measured every hour for 24 hours. After 24 h, 100 µL of 10% (v/v) Triton X100 solution was added, and the maximum fluorescence was determined. All experiments were performed in duplicate.

2.6. Evaluation of the photothermal conversion efficiency in solution

The photothermal efficacy of the formulations was measured in real-time during illumination using two K-type thermocouple probes. The liposomal suspensions (200 µM of PS) were placed 4 cm away from the laser diode before being illuminated for 10 min at 670 nm using an output power of 400 mW (fluence of ~800 mW/cm^2). The laser diode module was comprised of a laser diode driver and a temperature controller (LDM90, LDC220C, TED200C from Thorlabs Inc. Newton, New Jersey, United States). In order to check the reproducibility of the photothermal effect, three 10 min on / 15 min off cycles of illumination were carried out. The temperature increases (illumination on) and decreases (illumination off) for all 3 cycles were measured.

The process of nanoparticles-mediated photothermal hyperthermia can be described as a collective heating model.(Richardson et al., 2009) The photothermal conversion efficiency (η) can be calculated following the method described by Roper et al.(Roper et al., 2007) and reproduced by many other authors.(Chen et al., 2010; Jiang et al., 2013; Pattani and Tunnell, 2012; Zmerli et al., 2021a)

2.7. Evaluation of the generation of singlet oxygen

9,10-Anthracenediyl-bis(methylene)dimalonic acid (ABDA)-based oxidation method was used to assess the capability of PL-Por liposomes to generate $^1O_2$. (Wang et al., 2011) Water-soluble ABDA exhibits photobleaching when oxidized by $^1O_2$, which causes a decrease in ABDA absorption at 380 and 400 nm (maximum absorbance peak of ABDA). Suspensions of Ph_3LPC or Pyr_3LPC formulations (10 μM of PS) incubated with various concentrations of ABDA (10, 50 and 100 μM) were loaded in a quartz cell and placed 4 cm away from the laser diode. The suspensions were then illuminated for 10 minutes with a laser diode at a wavelength of 670 nm and an output power of 50 mW (fluence of ~100 mW/cm^2). The ABDA absorbance was recorded at 380 nm rather than the standard 400 nm to avoid the overlap between ABDA and the Soret band of the PL-Por conjugates (405 nm). The loss of absorbance at 380 nm after illumination for each mixture was plotted as a function of ABDA concentration.

2.8. In vitro PTT/PDT antibacterial experiments

2.8.1. Culture of bacteria

Bacteria strains used for the studies include Gram (+) *S. aureus* CIP4.83 and Gram (-) *P. aeruginosa* PAO1. Bacteria were grown in Lysogeny Broth (LB) (Peptone 10 g.L^{-1}, NaCl 10 g.L^{-1} and 5 g.L^{-1} of yeast extract). The bacterial strains were stored at -80 °C. For the preparation of planktonic cultures, single colonies were picked and inoculated in 10 mL of LB broth medium overnight at 37 °C at 160 rpm on an orbital shaker. Optical density (OD) of the bacterial suspension was determined by measuring the absorbance at 600 nm (OD_{600}). For the test with bacteria on stationary state of growth, the culture at OD_{600} = 0.2 were prepared with the first

preculture (OD_{600} = 5) and the samples were prepared with the same procedure as mentioned before.

2.8.2. Evaluation of the phototoxicity of the liposomes on planktonic culture

A new culture was started at OD_{600} = 0.05 by diluting 100 µL of the previous culture (~ OD_{600} = 5) in 10 mL of LB broth. The culture was incubated until an OD_{600} = 0.2 was recorded. An aliquot (100 µL) was removed from the OD_{600} = 0.2 solution and centrifuged for 5 min at 6000 rpm. The supernatant was removed and the pellet resuspended in autoclaved PBS (4 mL for *S. aureus* and 3 mL *P. aeruginosa*) to stop bacteria division. The phototoxicity was evaluated by incubating 200 µL of bacteria suspension (10^5 bacteria per mL) with Pyr_3LPC and Ph_3LPC liposomes suspensions (0.1µM, 1µM, 5µM and 10 µM) for 10 min. After incubation, the suspensions were illuminated for 10 minutes at 670 nm and 400 mW output power (fluence ~ 800 $mW.cm^{-2}$). After illumination, the suspension was serially diluted in PBS (10^{-1} to 10^{-4}) and 100 µL of each dilution was spread on LB petri dishes (LB + 15% of agar). The number of colony forming unit for each dilution was counted after 24 hours incubation at 37°C. In addition, control experiments of non-treated bacteria, bacteria illuminated for 10 min and Pyr_3LPC and Ph_3LPC liposomes without illumination were also carried out. CFU for each experiment was normalized to the non-treated control and plotted as concentration versus % cell viability. Each test was carried out in triplicate.

2.8.3 Evaluation of the phototoxicity of the liposomes on stationary phase planktonic cultures

The overnight cultures were diluted with PBS to an OD_{600} of 0.2. An aliquot (100 µL) was removed and centrifuged for 5 min at 6000 rpm. The PBS:LB supernatant was removed, and the

pellet resuspended in PBS (4 mL for *S. aureus* and 3 mL *P. aeruginosa*) to stop bacterial growth. The phototoxicity was evaluated by incubating 200 µL of bacteria suspension (approximately 10^5 bacteria per mL) with Pyr_3LPC and Ph_3LPC liposomes suspensions (1µM for *S. aureus* and 10 µM *P. aeruginosa*) for 10 min. After incubation the suspensions were illuminated for 10 minutes at 670 nm and 400 mW output power (fluence = 800 $mW.cm^{-2}$). After illumination, the suspension was serially diluted in PBS (10^{-1} to 10^{-4}) and 100 µL of each dilution was spread on LB petri dishes (LB + 15% of agar). The number of the colony forming unit for each dilution was counted after 24 hours of incubation at 37°C. In addition, control experiments of non-treated bacteria, bacteria illuminated for 10 minutes and Pyr_3LPC and Ph_3LPC liposomes without illumination were also carried out. CFU for each experiment was normalized to the non-treated control and plotted as concentration versus % cell viability. Each test was carried out in triplicate.

2.8.4 Evaluation of phototoxicity vs illumination time

A new culture was started at OD_{600} = 0.05 by diluting 100 µL of the previous culture (~ OD_{600} = 5) in 10 mL of LB broth. The culture was incubated until an OD_{600} = 0.2 was reached. An aliquot (100 µL) was removed from the OD_{600} = 0.2 suspension and centrifugated for 5 min at 6000 rpm. The supernatant was removed, and the pellet resuspended in PBS (4 mL for *S. aureus* and 3 mL *P. aeruginosa*) to stop bacteria replication. The phototoxicity was evaluated by incubating 200 µL of bacteria suspension (approximately10^5 bacteria per mL) with Pyr_3LPC and Ph_3LPC liposomes suspensions (5 µM) for 10 minutes. After incubation, the suspensions were illuminated for various times: 1, 5, 10 and 20 minutes at 670 nm and 400 mW output power (fluence ~ 800 $mW.cm^{-2}$). After illumination, the illuminated suspensions were serially diluted in PBS (10^{-1} to 10^{-4}) and 100 µL of each dilution was spread on LB petri dishes (LB + 15% of agar). The number of the colony forming unit for each dilution was counted after 24 hours of incubation

at 37°C. In addition, a control experiment where the bacteria were not illuminated was also carried out. CFU for each experiment was normalized to the non-illuminated control and plotted as concentration versus % cell viability. Each test was carried out in triplicate.

2.8.5 Growth of biofilms

Overnight cultures of *S. aureus* and *P. aeruginosa* were used to prepare 5 mL precultures in LB broth supplemented with 0.5% (w/v) glucose. Starting from OD_{600} = 0.05, the precultures were incubated until their optical density reached OD_{600} = 0.8. The whole culture was recovered and centrifuged at 4000 rpm for 15 minutes. The media was removed, and the pellet resuspended in 5 mL of PBS and centrifuged at 4000 rpm for 15 minutes. This washing step was repeated 3 times to completely remove any traces of the media. The resultant pellet was then resuspended in PBS (5 mL) and added to a petri dish with a confocal microscope slide (24 x 25 x 0.17 mm). The microscope slide was incubated with the bacteria suspension for 3 hours at 37°C to allow bacteria adhesion, the first step of biofilm formation. After incubation the bacteria suspension was removed and the microscope slide transferred to a new petri dish with 10 mL of LB media with 0.5% glucose and incubated for 72 h. For *S. aureus* biofilms, bacteria were incubated for *72* h without media change or agitation. Whereas, for *P. aeruginosa* biofilms, the bacteria were under agitation (100 rpm) and the culture medium was changed daily.

2.8.6 Phototoxicity effect on biofilms

Biofilms were incubated for 30 minutes with Pyr_3LPC or Ph_3LPC liposomes (100 μM of PS) suspensions diluted with PBS. The biofilms were illuminated for 10 minutes at 670 nm and 400 mW output power of (fluence = 800 $mW.cm^{-2}$). During illumination thermal images were taken using a Fluke Ti401 PRO thermal imager at 1 min and 5 min to observe the photothermal effects.

Pyr_3LPC or Ph_3LPC liposomes were removed, and the biofilm was washed with PBS (3 x 1 mL). The biofilm was then treated with Live/dead™ Backlight™ bacterial viability Kit (200 µL, SYTO9 (3.3 µM) and propidium iodide (20 µM) diluted in PBS) and left to incubate for 20 minutes in the dark. After incubation, slides were washed with PBS (3 x 1 mL). Each slide was then imaged on an inverted confocal SP8X microscope (Leica, Germany) using a HC PL APO CS2 10x air objective lens. The instrument was equipped with a WLL Laser and excitation wavelengths of 490 nm for SYTO9 and 560 nm for propidium iodide. Green and red fluorescence emission were collected respectively with a 500-550 nm (SYTO9) and a 560-620 nm (propidium iodide) wide emission slits under a sequential mode.

3. Results and discussion

3.1. Self-assembling properties of the lipid porphyrin conjugates

As described in our previous work(Bronstein et al., 2022b), Ph_xLPC and Pyr_xLPC conjugates could assemble into supramolecular structures with bilayers morphology and exhibited a diversity in shapes depending mainly on the type of the porphyrin core. Indeed, while Ph_xLPC assembled into closed ovoid structures, Pyr_xLPC formed rigid open sheets. However, only few structures that resemble to vesicles were observed (Bronstein et al., 2022b). By the mean of molecular dynamics simulations, we demonstrated that regardless of linker size, Ph_xLPC compounds exhibit less π-stacking events with respect to Pyr_xLPC ones and self assemble into less ordered lipid bilayers. In addition, Ph_xLPC had the tendency to form inter-leaflet π-stacked molecules, whereas Pyr_xLPC conjugates formed π-stacked molecules within the same leaflet, thus leading to a variety of different supramolecular morphologies. Hence, we hypothesized that reducing the π-π stacking interaction between the porphyrin cores by adding cholesterol may lead to the formation of stable

liposome-like assemblies as observed previously with other conjugates(Massiot et al., 2022; Massiot et al., 2018; Massiot et al., 2019). To do so, we mixed the conjugates with cholesterol at equimolar concentration in the presence of 5 mol % of DSPE-PEG_{2000}. Cholesterol may exhibit a complementary packing parameter to that of PL-Por conjugates and reduce the propensity of π-π stacking between the porphyrin cores that hinders the bilayer bending (Bronstein et al., 2022b). The presence of DSPE-PEG_{2000} in these formulations is mandatory to prevent the aggregation of the conjugate vesicles and the loss of material during the extrusion step. Moreover, DSPE-PEG_{2000} is usually used to prolong liposomes circulation time in the bloodstream, protecting them against opsonization, which could be beneficial for *in vivo* studies. Dynamic light scattering measurements for each liposomes formulation showed a monodisperse population with an average hydrodynamic diameter around 200 nm **(Table 1)** depending on the PL-Por conjugate.

Formulations	**Hydrodynamic diameter (nm)**	**PdI**	**λ_R (nm)**	**Fluorescence quenching percentage (%)**
Pyr_2LPC:Chol:DSPE-PEG_{2000}	204 ± 9	0.18 ± 0.03	8	94 ± 7
Pyr_3LPC:Chol:DSPE-PEG_{2000}	187 ± 4	0.07 ± 0.04	8	97 ± 4
Pyr_4LPC:Chol:DSPE-PEG_{2000}	187 ± 12	0.08 ± 0.03	8	99 ± 1
Ph_2LPC:Chol:DSPE-PEG_{2000}	176 ± 4	0.10 ± 0.04	8	96 ± 2
Ph_3LPC:Chol:DSPE-PEG_{2000}	182 ± 7	0.20 ± 0.02	8	96 ± 2
Ph_4LPC:Chol:DSPE-PEG_{2000}	181 ± 5	0.02 ± 0.01	8	95 ± 4

Table 1: Properties of Ph_xLPC and Pyr_xLPC assemblies (PL-Por: Chol: DSPE-PEG_{2000}, 47.5:47.5:5 mol%). Formulation compositions, size measured by DLS with the corresponding polydispersity index (PdI), fluorescence quenching percentage [(1- (F_0 /F_{det}))×100] where F_0 is the fluorescence of the PS at 675 nm in the intact vesicles, and F_{det} is the fluorescence signal after addition of 1% of Triton X-100) and λ_R is the red-shift observed on the absorbance spectra before disruption of the nanoassemblies.

As depicted in **Figure 1**, the six conjugates could form liposomal structures with the presence of lipid bilayer exhibiting an average thickness of ~ 5 nm, which is consistent with the thickness reported previously by Massiot *et al.* (Massiot et al., 2022; Massiot et al., 2018; Massiot et al., 2019) and Lovell *et al.* (Lovell et al., 2011).

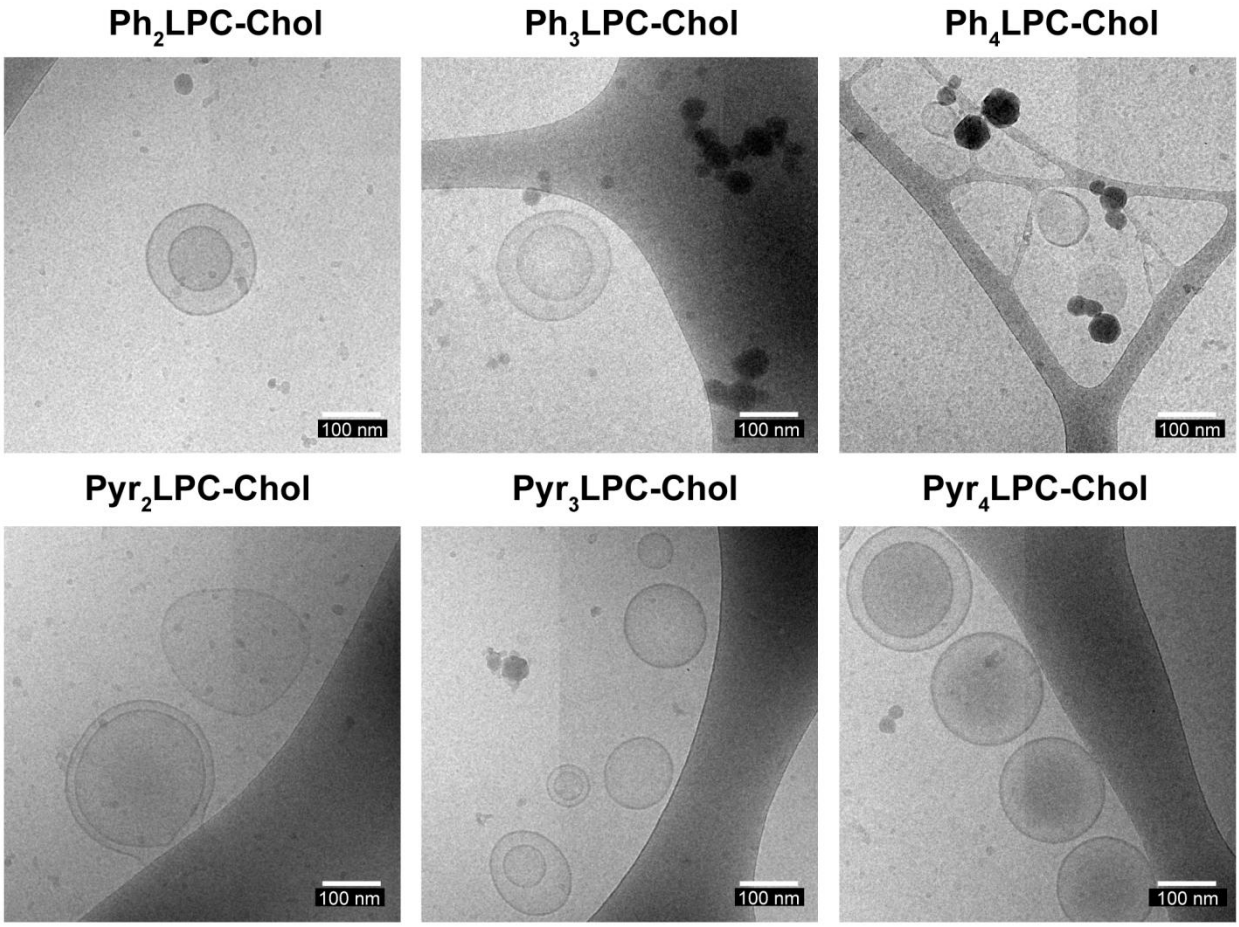

Figure 1. Cryo-TEM images of each lipid-porphyrin conjugates formulation with cholesterol and DSPE-PEG_{2000} (47.5:47.5:5).

3.2. Photophysical properties of the assemblies

The optical properties were then evaluated for all six formulations by absorbance and fluorescence intensity measurements. As shown in **Figure 2, S1 and S2**, the formulations made of Ph_xLPC or Pyr_xLPC with cholesterol exhibited different absorbance features than their monomeric counterparts. In fact, independently of the porphyrin core and the lipid backbone, all

formulations exhibited a damping of the Soret and the Q_{max} bands with a slight red shift (~8 nm) of the latter. Such behavior could indicate that both Ph_xLPC and Pyr_xLPC based assemblies form disordered porphyrin-porphyrin aggregates. Moreover, despite the higher molar ratio of Pyr_xLPC in these formulations, we did not observe the large red shift indicative of ordered J- aggregates (Shakiba et al., 2016), as observed previously with the pure Pyr_xLPC assemblies(Bronstein et al., 2022b). We attributed this absence of J-aggregates to the large amount of Chol in the formulations, which could reduce the interactions between the porphyrins cores required to form ordered J-aggregates. However, both Ph_xLPC and Pyr_xLPC assemblies displayed extensively quenched fluorescence compared to the corresponding monomers released following solubilization with 1 vol % of Triton X100. The fluorescence quenching percentage was calculated and is reported in Table 1. Each lipid-porphyrin conjugate formulation reported a quenching fluorescence percentage superior to 90%. Similar behavior has been observed by Lovell *et al.* when they formulated pyro-lipid with cholesterol at 30 mol% and reported a quenching percentage ~99% (Lovell et al., 2011). Such fluorescence quenching is related to the strong interactions between porphyrins inside the nanoassemblies and highlights their use as a potential photothermal agent. Yet, we noticed that Pyr_xLPC formulations displayed a slightly higher quenching fluorescence compared to Ph_xLPC formulations. This difference in quenching could be attributed to the difference of structure between Pyr_xLPC and Ph_xLPC conjugates. As demonstrated in our previous works (Bronstein et al., 2022b), Pyr_xLPC conjugates exhibited stronger π-π interaction between the porphyrin cores compared to Ph_xLPC conjugates which allowed them to form more ordered aggregates when they assembled. The better stacking properties of the Pyr_xLPC conjugates led to more organized porphyrin-porphyrin aggregates with

a better fluorescence quenching percentage and should provide higher photothermal conversion efficiency compared to Pheo-a conjugates.

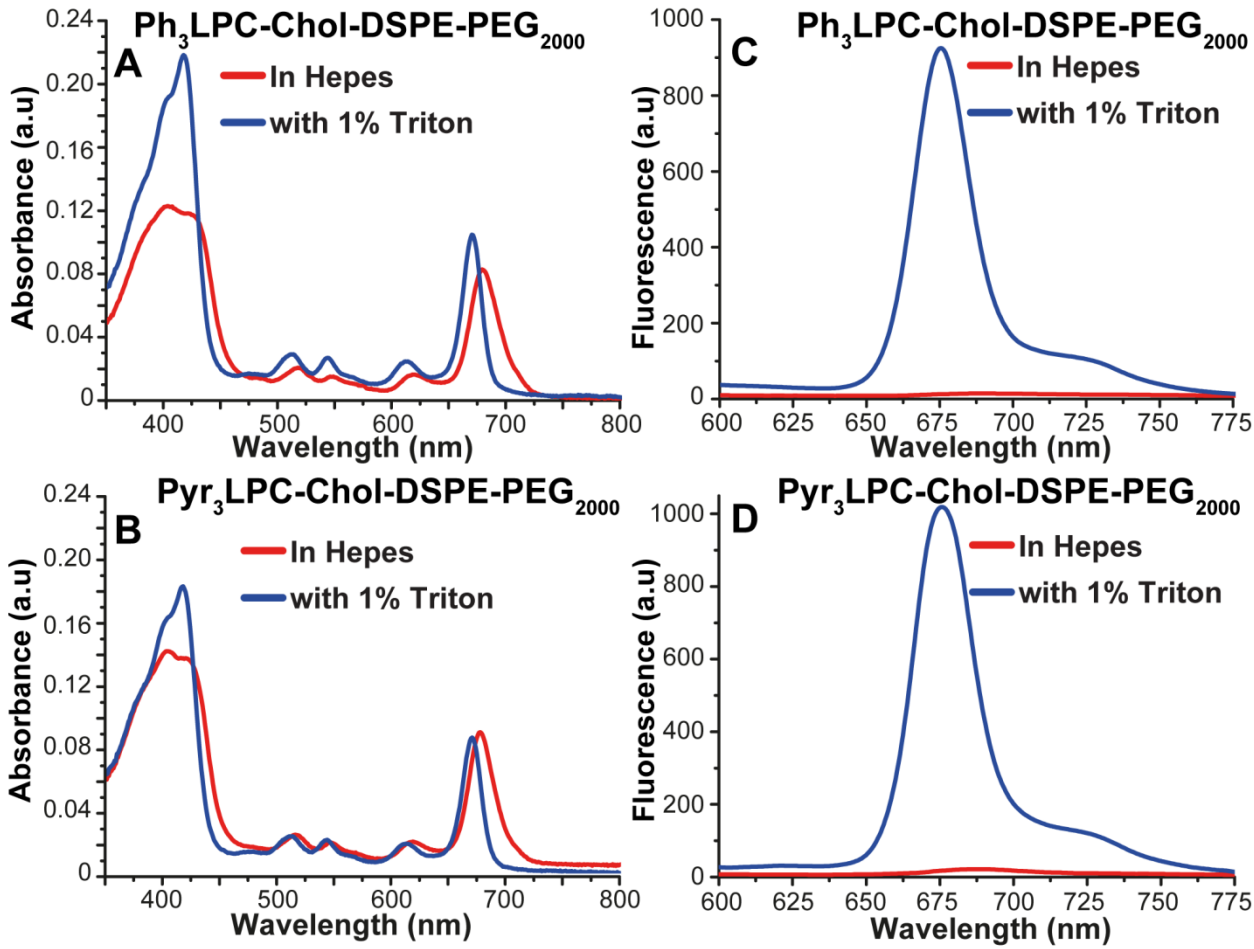

Figure 2. Absorbance (A, B) and Fluorescence (C, D) spectra of Ph_3LPC:Cholesterol:DSPE-PEG_{2000} (47.5:47.5:5) and Pyr_3LPC:Cholesterol:DSPE-PEG_{2000} (47.5:47.5:5) liposomes before (red line) and after (blue line) addition of 1% Triton X100.

3.3. Stability of the assemblies in biological medium

The stability of liposomal formulations is a key issue for their use as a drug delivery system in clinical applications. The adsorption of serum proteins at the surface of lipid-porphyrin conjugate nanoassemblies can destabilize their structure. This in turn will alter their pharmacokinetics and their photophysical properties. The photothermal effect of our formulations is the result of an

intense fluorescence quenching due to a tight packing and interactions between lipid-porphyrin conjugates when assembled. So, the stability of our formulations could be inferred from the quenching efficiency because the fluorescence is recovered upon dissociation into monomers. If the assemblies are unstable in serum they should display rapid decay of their fluorescence quenching efficiency. To assess their stability, each formulation was incubated for 24 h in the presence of 10% (v/v) fetal bovine serum (FBS) at 37°C. The fluorescence of the assemblies was measured every hour for 24 h and they were finally disrupted with 1% triton X100 to regenerate the total fluorescence. As shown in **Figure 3**, **S3 and S4**, Ph_xLPC liposomal formulations displayed a continuous increase in the fluorescence over 24 h. Such behavior results from the gradual dissociation of the assemblies into monomers and the regeneration of monomers fluorescence. For these formulations, the fluorescence increase was already observed after 1h incubation which implies their rapid interaction and destabilization by serum proteins. Indeed, we noticed that the percentages of regenerated fluorescence after 24 hours were 63% for Ph_2LPC, 45% for Ph_3LPC and 33% for Ph_4LPC. The stability of the assemblies was related to the PL-Por conjugate structure, increasing with the length of the linker separating the porphyrin core from the phospholipid derivative. The dramatic increase in stability observed for Ph_4LPC assemblies could be due to the longer linker which allows for a better match between the sn1 and sn2 alkyl chains, and allows the conjugate to be firmly embedded in the bilayer. Inversely, Ph_2LPC has a shorter sn2 chain and thus presents a mismatch between the sn1 and sn2 alkyl chains, which could lead to it being loosely held in the bilayer. The same trend was observed for Pyr_XLPC conjugates. Indeed, the percentages of regenerated fluorescence after 24 hours were 28% for Pyr_2LPC, 12% for Pyr_3LPC and 9% for Pyr_4LPC, which strengthens our hypothesis. Obviously, Pyr_xLPC conjugates displayed a better stability in biological media compared to their pheophorbide-a analogs (**Figure S5**). These results may be attributed once again to the better

stacking properties of Pyr_xLPC conjugates which form nanoassemblies with a tighter organization around the porphyrin and make them harder to destabilize than the Ph_xLPC nanoassemblies.

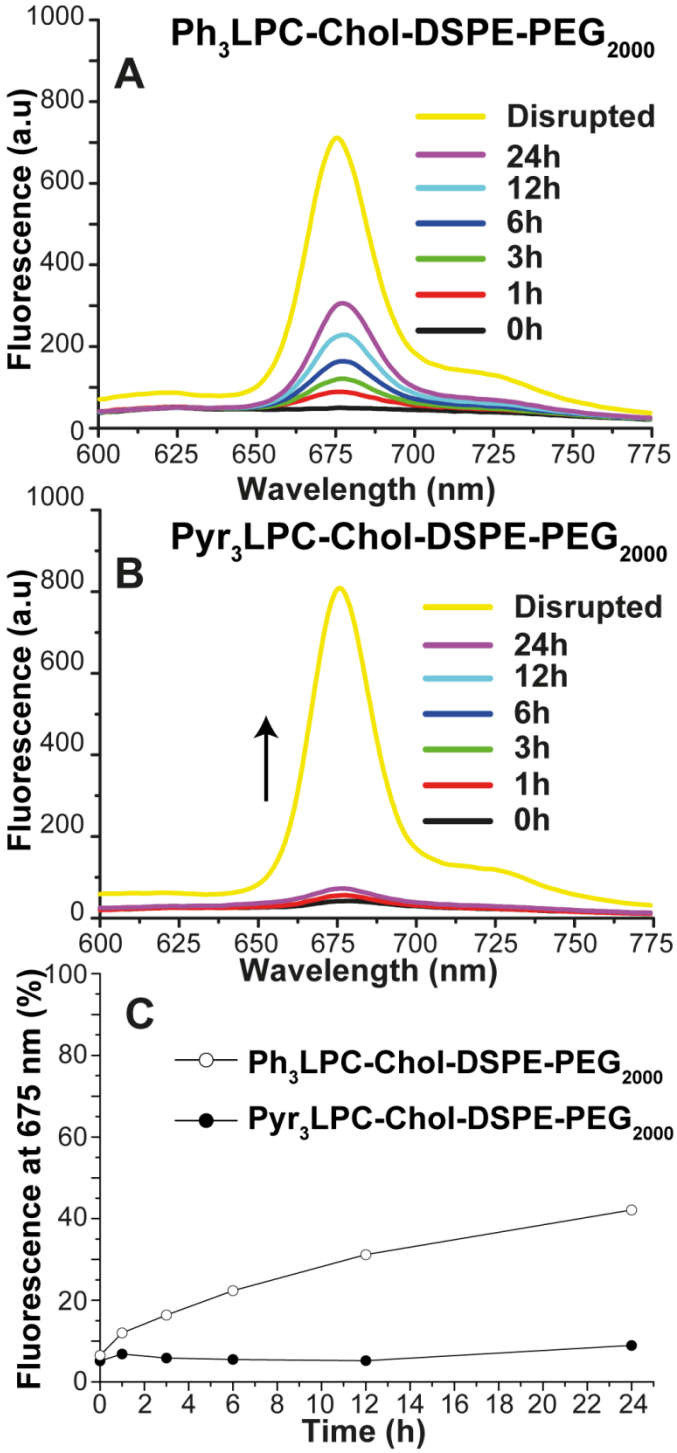

Figure 3. Stability of Ph_3LPC and Pyr_3LPC formulations in biological medium (10% FBS (v/v), 37°C) over 24 h. Fluorescence spectra of (A) Ph_3LPC and (B) Pyr_3LPC formulations: 0 h (black), 1 h (red), 3 h (green), 6 h (marine blue), 12 h (light blue), 24 h (purple) and finally disrupted with the addition of 1% triton X-100 (yellow). (C) Graph representing the regenerated fluorescence at 675 nm of Pyr_3LPC and Ph_3LPC formulations. The percentage of regenerated fluorescence is calculated by dividing the fluorescence intensity at 675 nm of each spectrum at every hour by the fluorescence intensity of the same formulation measured after disruption with Triton X100.

Since all Ph_xLPC and Pyr_xLPC formulations could form stable assemblies and in order to evaluate the impact of the porphyrin core on their photothermal / photodynamic activities against bacteria, Ph_3LPC and Pyr_3LPC formulations were chosen as potential candidates for assessment of the antibacterial properties.

3.4. Assessment of the photothermal and photodynamic properties of the assemblies

The stability of an organic NIR photothermal agent is crucial for biomedical applications, where longer time illumination, or repeated illumination cycles are needed. So, we investigated the photothermal properties of the Pyr_3LPC and Ph_3LPC (200 μM of PS) nano-assemblies over multiple heating cycles. To do this, we monitored the temperature increase during illumination (10 min, 400 mW, fluence 800 $mW.cm^{-2}$) using thermocouple probes. The vesicles suspensions were subjected to three consecutive laser illumination cycles with 15 min of cooling between each illumination. As depicted in **Figure 4**, the temperature of the vesicle suspensions increased nonlinearly upon laser irradiation until reaching a steady state after 10 minutes. The heating cycle was followed by a 15 min cooling period. A temperature increase over room temperature (ΔT) of 18.4 °C for Ph_3LPC liposomes and 20.6°C for Pyr_3LPC liposomes was obtained. The heat conversion efficiency was also calculated following the procedure outlined by Roper et al. (Roper et al., 2007) and was found to be 30% and 37% for Ph_3LPC and Pyr_3LPC, respectively (**Figure 4**), which is in line with other organic PTT agents (Jung et al., 2018). The photothermal conversion efficiencies of both PL-Por formulations are in line with other lipid-porphyrin

conjugates such as Pyrolipid (Charron et al., 2020) and PhLSM when mixed with cholesterol at equimolar percentage .(Massiot et al., 2022) This result shows that both Ph_3LPC and Pyr_3LPC conjugates are suitable PTT agents. While it is worth noting that for the Pyr_3LPC formulation, the heating cycles were fully reproducible indicating good photothermal stability over the 3 cycles of illumination, the same cannot be said for the Ph_3LPC liposomes for which we observed a decrease in the ΔT during the subsequent heating cycles. This could be explained by a partial photo-bleaching of the Ph_3LPC conjugate over the 3×10 min of illumination. This hypothesis is supported by work by Charron *et al*. (Charron et al., 2020) and *Massiot et al. (Massiot et al., 2022)* who reported that the formation of disordered aggregates in phospholipid-porphyrin conjugates assemblies does not completely prevent the generation of singlet oxygen when they are illuminated, and the generated singlet oxygen could result in porphyrin photobleaching. (Berg et al., 2005) We reported in the fluorescence experiments that Ph_3LPC conjugate display a lower fluorescence quenching compared to their Pyr_3LPC analogue. Therefore, the lesser reproducibility of the heating cycles could be due to the Ph_3LPC being less fluorescence quenched and generating more singlet oxygen upon illumination resulting in a higher degree of photobleaching.

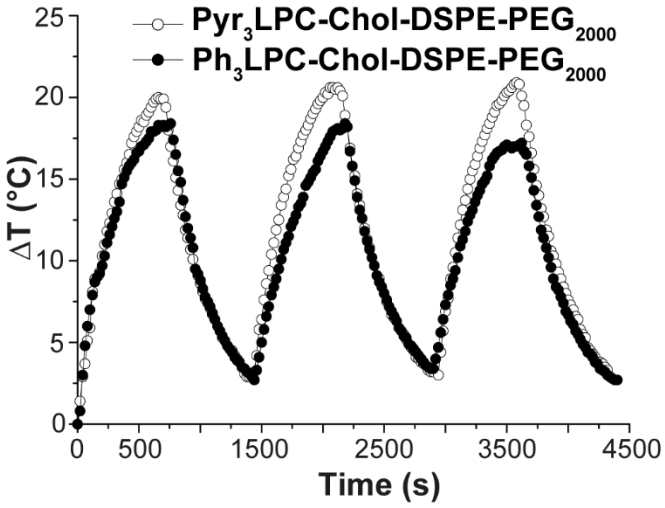

Formulations	ΔT_{max} (°C)	η
Pyr_3LPC-Chol-DSPE-PEG_{2000}	20.6 ± 0.4	37 %
Ph_3LPC-Chol-DSPE-PEG_{2000}	18.4 ± 1.9	30 %

Figure 4. (A) Photothermal effect of Ph_3LPC:Cholesterol :DSPE-PEG_{2000} and Pyr_3LPC:Cholesterol :DSPE-PEG_{2000} (47.5 :47.5 :5) liposomes with a final PS concentration of 200 μM. Liposomes were illuminated with a 670 nm laser diode at a fluence of 800 mW.cm^{-2} for 10 min. After illumination the sample was allowed to cool for 15 min (laser turned off), this cycle of heating and cooling was repeated three times. The increase in temperature observed for each formulation was plotted as the difference with initial temperature of each formulation (ΔT). (B) Table summarizing the maximum temperature increase (ΔT_{max}) and the heat conversion efficiency (η) for the studied Ph_3LPCand Pyr_3LPC formulations.

To further confirm our hypothesis that Ph_3LPC liposomes generate more singlet oxygen when illuminated, we carried out an ABDA-oxidation experiment.(Ikeda et al., 2017) ABDA is used as a probe for detecting singlet oxygen in solution as it reacts both rapidly and selectively with $^1O_2$. The oxidation of ABDA by singlet oxygen causes a dramatic photobleaching **Figure 5 (A)**, which was monitored by UV-vis spectrometry after 10 min irradiation (670 nm, 100 mW.cm^{-2}). Any decrease in ABDA absorbance was also monitored (380 nm). Mixtures of Ph_3LPC or Pyr_3LPC liposomes and ABDA (10:10, 10:50 and 10:100 μM (PL-Por: ABDA)) were made and the difference of ABDA absorbance at 380 nm before and after 10 min irradiation was calculated and plotted as a function of ABDA concentration (**Figure 5B**).

As depicted in Figure 5B, we notice for both formulations a higher loss in absorbance at 380 nm at the highest ratios of ABDA. This could be explained by the fact that as the quantity of ABDA in the mixture increases, the probability for the short-lived singlet oxygen (3-4 μs)(Sharman et al., 2000) to interact with an ABDA molecule increases. This will increase the quantity of oxidized ABDA molecules. Moreover, the extent of absorbance loss at 380 nm increases linearly with the ABDA concentration in the mixture which means that some of the singlet oxygen generated is still not reacting with ABDA. Interestingly, at equal concentration in the mixture (10 μM, PS) Ph_3LPC formulations (black squares) demonstrate a more significant loss in absorbance than Pyr_3LPC liposomes (red circle) at all the concentrations of ABDA tested. Such result can be related either to the higher inner photodynamic efficiency of Ph_3LPC compared to Pyr_3LPC or to different extent of packing of the conjugates inside the assemblies. In order to verify our hypothesis, we have repeated the ABDA-oxidations experiment but in ethanol where both conjugates are soluble. As shown in Figure S6 and in contrary to the experiments performed with the assemblies, Pyr_3LPC conjugates in ethanol exhibit higher photodynamic efficiency than Ph_3LPC. We can therefore assume that the Ph_3LPC conjugates are less packed inside the assemblies compared to Pyr_3LPC ones which offer them more oxidative capacity than Pyr_3LPC ones. This result confirms our hypothesis from the PTT data that Ph_3LPC liposomes can generate relatively more ROS than Pyr_3LPC liposomes.

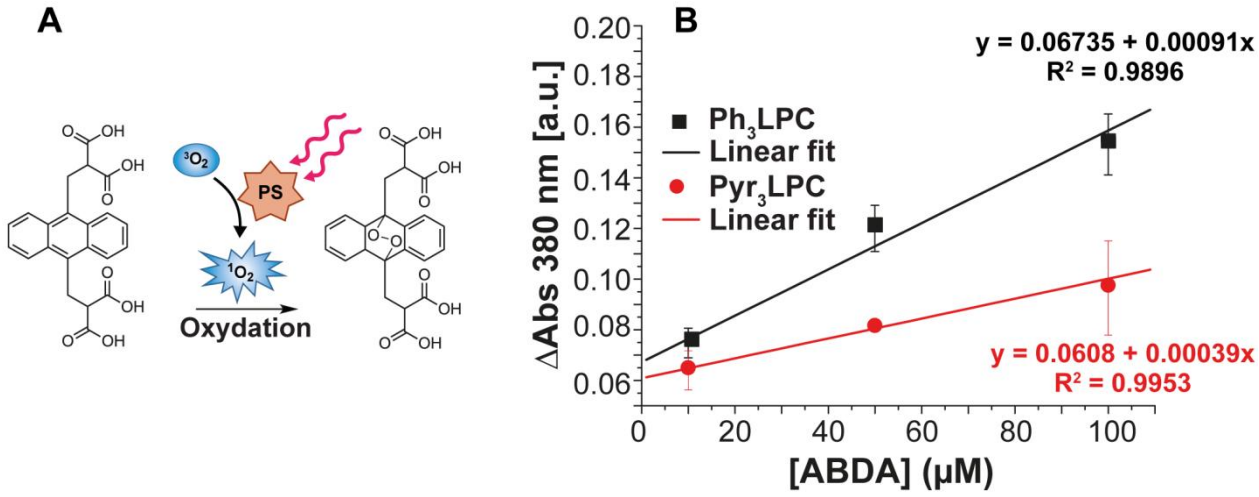

Figure 5. Evaluation of singlet oxygen generation of Ph_3LPC and Pyr_3LPC liposomes. (A) Schematic representation of the ABDA oxidation following its reaction with singlet oxygen. (B) Ph_3LPC and Pyr_3LPC liposomes (10 μM in PS) were incubated with various amount of ABDA (10, 50 and 100 μM). The absorbance of ABDA at 380 nm was measured before and after 10 minutes of illumination (670 nm, 100 $mW.cm^{-2}$). The loss in absorbance at 380 nm was calculated and plotted as a function of ABDA concentration.

3.5. Antimicrobial effect on Planktonic cultures of Pyr_3LPC and Ph_3LPC liposomes

The PTT/PDT antibacterial activity of Ph_3LPC and Pyr_3LPC liposomes was tested against *P. aeruginosa* (Gram (-)) and *S. aureus* (Gram (+)). *P. aeruginosa* and *S. aureus* were incubated with different concentrations of Ph_3LPC and Pyr_3LPC liposomes: 0.1, 1, 5 and 10 μM and then illuminated at 670 nm for 10 min (400 mW, fluence 800 $mW.cm^{-2}$). Their ability to kill bacteria populations was assessed using a basic spread plate method (Hartman). We observed that irradiation with the laser alone had no significant impact on the viability of both strains (see **Figure S7**). To determine the optimal illumination time required for an effective bactericidal efficacy, we illuminated both strains in the presence of Ph_3LPC and Pyr_3LPC (10 μM) for varying times: 1, 5, 10 and 20 min. From this experiment it was determined that 10 min was a suitable illumination time to observe the maximum toxic effect for both bacterial strains (**Figure S7)**. Moreover, after 10 min illumination a plateau of the photothermal effect was reached. Next, we tested the toxicity of Ph_3LPC and Pyr_3LPC in the dark, as PDT/PTT agents should be

nontoxic unless illuminated. Therefore, we incubated both strains with Ph_3LPC and Pyr_3LPC (10 μM) for 1 h before carrying out the basic spread plate method. Neither Ph_3LPC nor Pyr_3LPC exhibited significant antibacterial activity even at the highest concentration of 10 μM when incubated in the dark (**Figure 6**). Interestingly, as shown in **Figure 6**, upon the illumination of the bacterial suspensions incubated with Ph_3LPC and Pyr_3LPC, a significant antibacterial effect was observed. Moreover, the phototoxicity against both strains increased with the concentrations of Ph_3LPC and Pyr_3LPC.

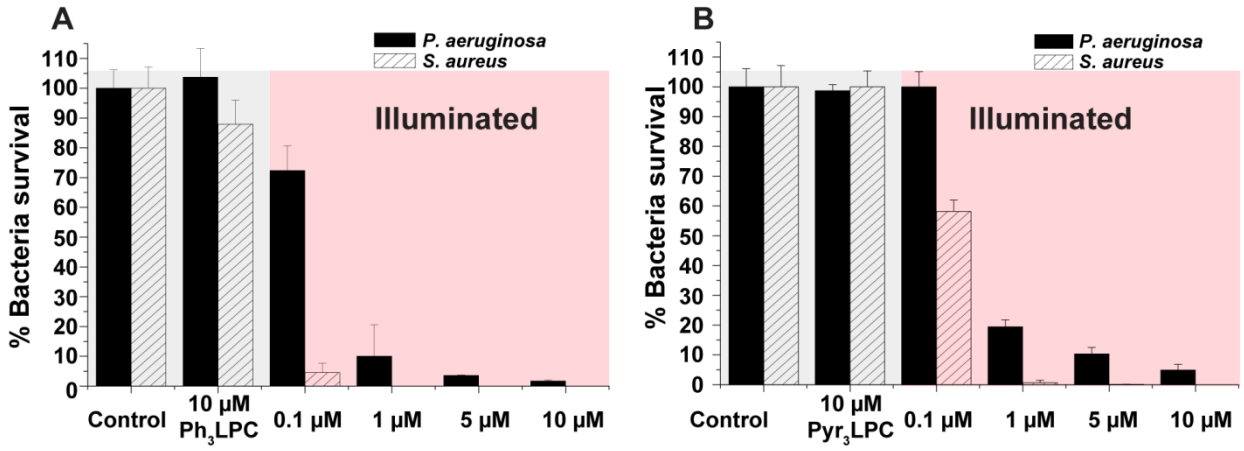

C

	S. aureus		*P. aeruginosa*	
IC_{90} (μM)	**Pyr_3LPC**	0.66 ± 0.01	**Pyr_3LPC**	5.45 ± 1.42
	Ph_3LPC	< 0.1	**Ph_3LPC**	1.63 ± 1.02

Figure 6. Antimicrobial effects of Ph_3LPC (A) and Pyr_3LPC (B) liposomes (0-10 μM) on *S. aureus* (stripped) and *P. aeruginosa* (black) planktonic cultures with and without (Ph_3LPC or Pyr_3LPC controls) 10 min of illumination (670 nm, 800 $mW.cm^{-2}$). (C) Table summarizing the IC_{90} of the two formulations against *S. aureus* and *P. aeruginosa* populations. Each measurement is an average of three independent experiments (n= 3).

For *S. aureus*, we observed that both formulations were very effective with IC_{90} values (concentration required to kill 90% of the bacteria population)(Sun et al., 2016) less than 1 μM. All concentrations above these values resulted in a complete eradication of the bacteria. For

Ph_3LPC, the IC_{90} was below 100 nM whereas Pyr_3LPC exhibited an IC_{90} of 660 nM (**Figure 6 (C)**). These results demonstrate that both molecules possess an excellent antibacterial effect against gram (+) bacteria with a better effect for Ph_3LPC liposomes. This could be related to the difference in the photodynamic efficiency between Ph_xLPC and Pyr_xLPC. This trend in toxicity was also observed in *P. aeruginosa* where the IC_{90} values were 5.45 μM and 1.63 μM for Pyr_3LPC and Ph_3LPC, respectively (**Figure 6 (C)**). The increase in the IC_{90} for *P. aeruginosa* over *S. aureus* could be attributed to the different cell wall architecture between Gram (-) (*P. aeruginosa*) and Gram (+) (*S. aureus*) bacteria which makes them more resistant to several treatments such as aPDT. Indeed, the cell wall of Gram (-) bacteria exhibits a more complex structure compared to Gram (+) bacteria, which includes the presence of an outer lipid bilayer membrane that surrounds the peptidoglycan of the periplasmic part. This structural organization forms a physical and functional barrier that hinders the incorporation of PS into the inner membrane, limiting the photodynamic and photothermal therapies ability to kill Gram (-) bacteria.(Hamblin and Hasan, 2004) However, complete bacteria eradication of Gram (-) bacteria can still be achieved with aPDT by using higher concentrations of PS, implementing longer illumination times or increasing the power of the illumination source (Street et al., 2009).

The two formulations were also tested on the *S. aureus* and *P. aeruginosa* in the stationary state of growth using the same protocol. Bacteria in stationary phase change their metabolic state and consequently are known to be more resistant to antibacterial treatment especially to antibiotics (Reygaert, 2018). Cells with a low level of activity (sometimes called persisters) represent often an important part of the total population that constitute a biofilm and are one of the reasons for their well-documented resistance to conventional antibiotic treatments (Costerton et al., 1999; Lebeaux et al., 2014; Mah and O'Toole, 2001; Stewart, 2002). Both strains were treated at sub-

eradication concentrations so that any increase in their survival could be observed. Therefore, *S. aureus* and *P. aeruginosa* were treated with Ph_3LPC or Pyr_3LPC liposomes at 1 μM PS and 10 μM PS, respectively. We observed that for both *S. aureus* and *P. aeruginosa* the phototoxicity of Ph_3LPC and Pyr_3LPC was not affected by the growth state of the bacteria (**Figure S9**). These results agree well with studies of other photothermal/photodynamic agents reported in the literature, which have shown that PDT and PTT are effective at killing bacteria independently of their state of growth.(Banfi et al., 2006) From these experiments, we observe that both Pyr_3LPC and Ph_3LPC possess an excellent antibacterial effect on both strains with Ph_3LPC being the superior agent. The differences in toxicity may be attributed to the better oxidative power of Ph_3LPC compared to Pyr_3LPC demonstrated in the previous section, which could lead to Ph_3LPC exhibiting a stronger photodynamic effect.

3.5. Antimicrobial effects of Ph_3LPC and Pyr_3LPC liposomes on biofilms

We then explored the application of Ph_3LPC and Pyr_3LPC liposomes to *S. aureus* and *P. aeruginosa* biofilms. Biofilms were grown for 72 h before being incubated for 30 min with Ph_3LPC or Pyr_3LPC liposomes (100 μM PS) and further treated with or without NIR laser irradiation (10 min, 670 nm, fluence 800 $mW.cm^{-2}$). The ability of Ph_3LPC and Pyr_3LPC to damage biofilms was evaluated qualitatively by confocal fluorescence microscopy using the LIVE/DEAD biofilm viability assay. In this assay the Syto9 crosses intact membranes and stains nucleic acids whereas propidium iodide (PI) is not able to pass an intact membrane and therefore stains only the nucleic acids (DNA and RNA) of dead cells or cells with compromised membrane.

S. aureus is often involved in biofilm associated infections and their extracellular matrix is composed of polysaccharides, proteins and eDNA(Bao et al., 2015; Sugimoto et al., 2018; Wei and Ma, 2013) and a Tn-seq approach has allowed to identify genes necessary for eDNA release(DeFrancesco et al., 2017). When DnaseI is added to a biofilm, the matrix biomass is reduced attesting of the crucial role of eDNA in its structure. *P. aruginosa* has been used as a model for the formation of biofilm. In the *P. aruginosa* strain, eDNA is released by the action of a bacteriophage related lysine and holin and is critical for the viscoelasticity properties of the biofilm (Seviour et al., 2021). Therefore, when using PI, it is not surprising to observe a "red" background and a lot of "red" cells in 72 h old biofilms of *P aeruginosa* and *S. aureus*. Indeed, as documented recently by Rosenberg *et al.(Rosenberg et al., 2019)*, PI surestimates the cellular mortality by staining eDNA. But the qualitative analysis of the merge (PI + Syto9) images with increasing PI staining after treatment (compared to controls) remains a good indicator of the efficiency of the treatment. In **Figure 7 (B)** and **Figure 8 (B)**, the laser irradiation alone had no significant impact on both *P. aeruginosa* and *S. aureus* biofilms. Indeed, the resultant merged fluorescence images were predominantly green and comparable to the non-treated controls. The results for *S. aureus* biofilms have been reported in **Figure 7**. **Figure 7 (C) and (E)** indicate that both Ph_3LPC and Pyr_3LPC have negligible effect on the biofilm in the absence of light. Conversely, when Ph_3LPC or Pyr_3LPC were illuminated by NIR light for 10 min, the LIVE/DEAD™ images showed an intense red fluorescence indicating a significant increase in nucleic acids accessible for staining with PI, meaning dead bacteria or at least damaged membranes. These results agree with the planktonic toxicity data which suggested that both Pyr_3LPC and Ph_3LPC liposomes are effective antimicrobial photothermal and photodynamic agents. Interestingly, thermal images were taken during the laser illumination and reported in **Figure S10**. In addition, using a photothermal camera, we observed a maximal increase in

temperature to 42-45°C (ΔT~24°C) following the illumination of both formulations which corresponds to a mild hyperthermia (Ibelli et al., 2018). These results confirm the ability of PL-Por assemblies to generate combined photodynamic and photothermal effects on biofilms. Taken together, these data show that when Ph_3LPC or Pyr_3LPC assemblies are illuminated at a wavelength of 670 nm, they act as effective and efficient PT/PD agents and have a significant impact on the viability of *S. aureus* biofilms (**Figure 7 (D)** and **(F)**).

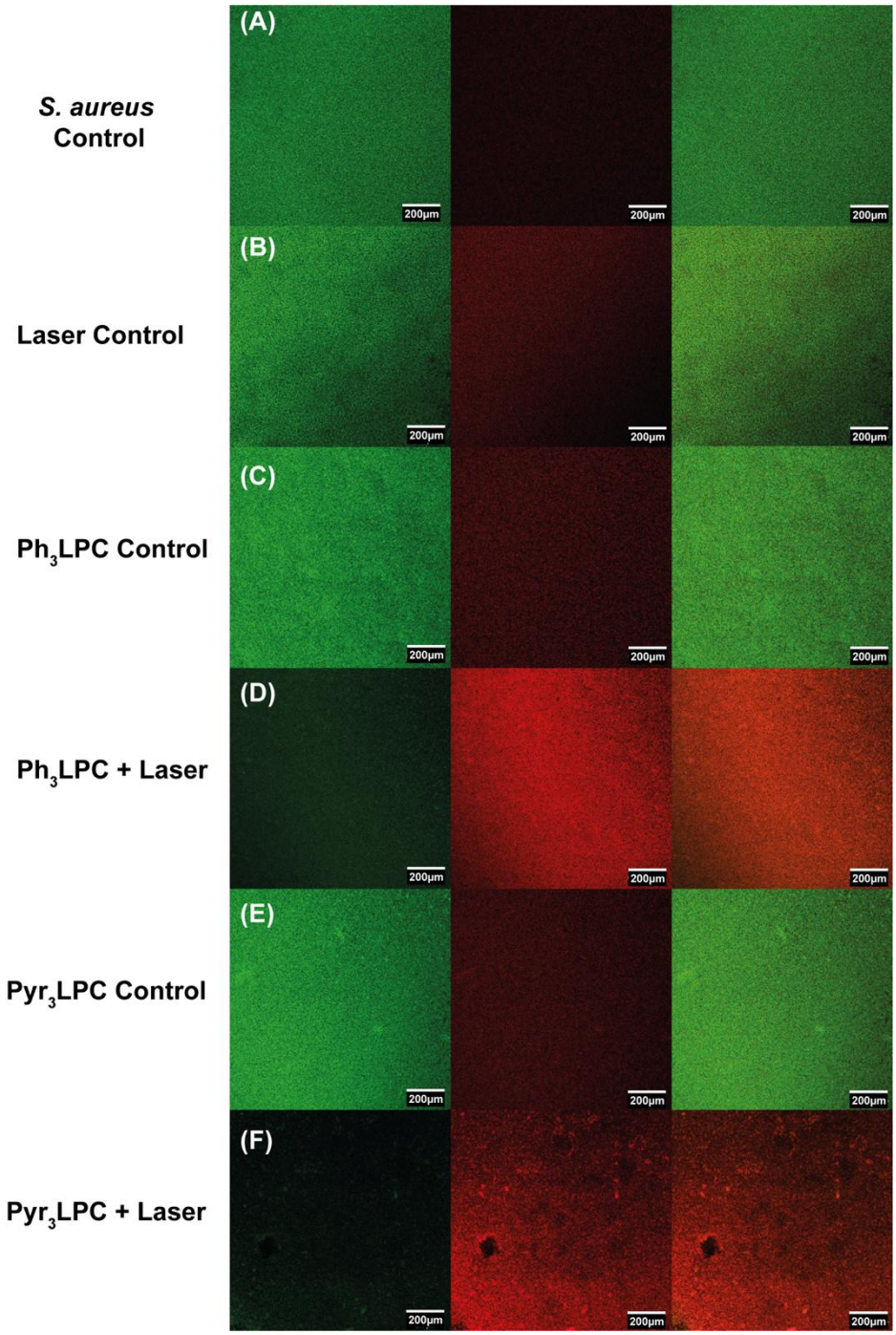

Figure 7. Confocal microscopy images of *S. aureus* biofilms treated with the LIVE/DEAD™ BacLight Bacterial viability Kit. Green images correspond to live bacteria (Syto9, left) and red ones to dead bacteria (PI, middle), while the right column is a merged image of both green and red channels. (A) *S. aureus* biofilm treated with PBS (control). (B) *S. aureus* biofilm after 10 min irradiation (laser control, 670 nm, 800 mW.cm^{-2}). (C) *S. aureus* biofilm treated with Ph_3LPC liposomes (100 µM PS) without laser irradiation. (D) *S. aureus* biofilm treated with Ph_3LPC liposomes (100 µM PS) with 10 min irradiation (670 nm, 800 mW.cm^{-2}). (E) *S. aureus* biofilms treated with Pyr_3LPC liposomes (100 µM PS) without laser irradiation. (F) *S. aureus* biofilms treated with Pyr_3LPC liposomes (100 µM PS) with 10 min irradiation (670 nm, 800 mW.cm^{-2}). The scale bar is 200 µm.

Regarding *P. aeruginosa* biofilms, **Figure 8 (C) and (E)** indicate that both Ph_3LPC and Pyr_3LPC assemblies have no toxic effect in the dark. When the biofilms were treated with both Pyr_3LPC and Ph_3LPC and red light the fluorescence images showed some increase in dead bacteria (red fluorescence) but a moderate amount of green fluorescence remained, indicating that the *P. aeruginosa* biofilm was not completely eradicated at this concentration. This suggests that both molecules are less effective on *P. aeruginosa* than on *S. aureus*. Ph_3LPC liposomes exhibit a more intense red fluorescence than Pyr_3LPC suggesting a better antibiofilm activity against *P. aeruginosa* which confirms the planktonic evaluation where the concentration on Pyr_3LPC had to be multiplied by 5 to get a similar effect on *P. aeruginosa* culture. Furthermore, **Figure S10** also confirms the photothermal effect of Pyr_3LPC and Ph_3LPC following their illumination by inducing mild hyperthermia temperature 42-45°C ($\Delta T \sim 24°C$).

Altogether, Ph_3LPC and Pyr_3LPC liposomes display both an effective antimicrobial and antibiofilm activity on Gram (+) bacteria based on combined PDT/PTT effects. Gram (-) bacteria require higher concentration of Ph_3LPC and Pyr_3LPC liposomes to obtain a similar effect on both planktonic bacteria and biofilms vs their Gram (+) analogs.

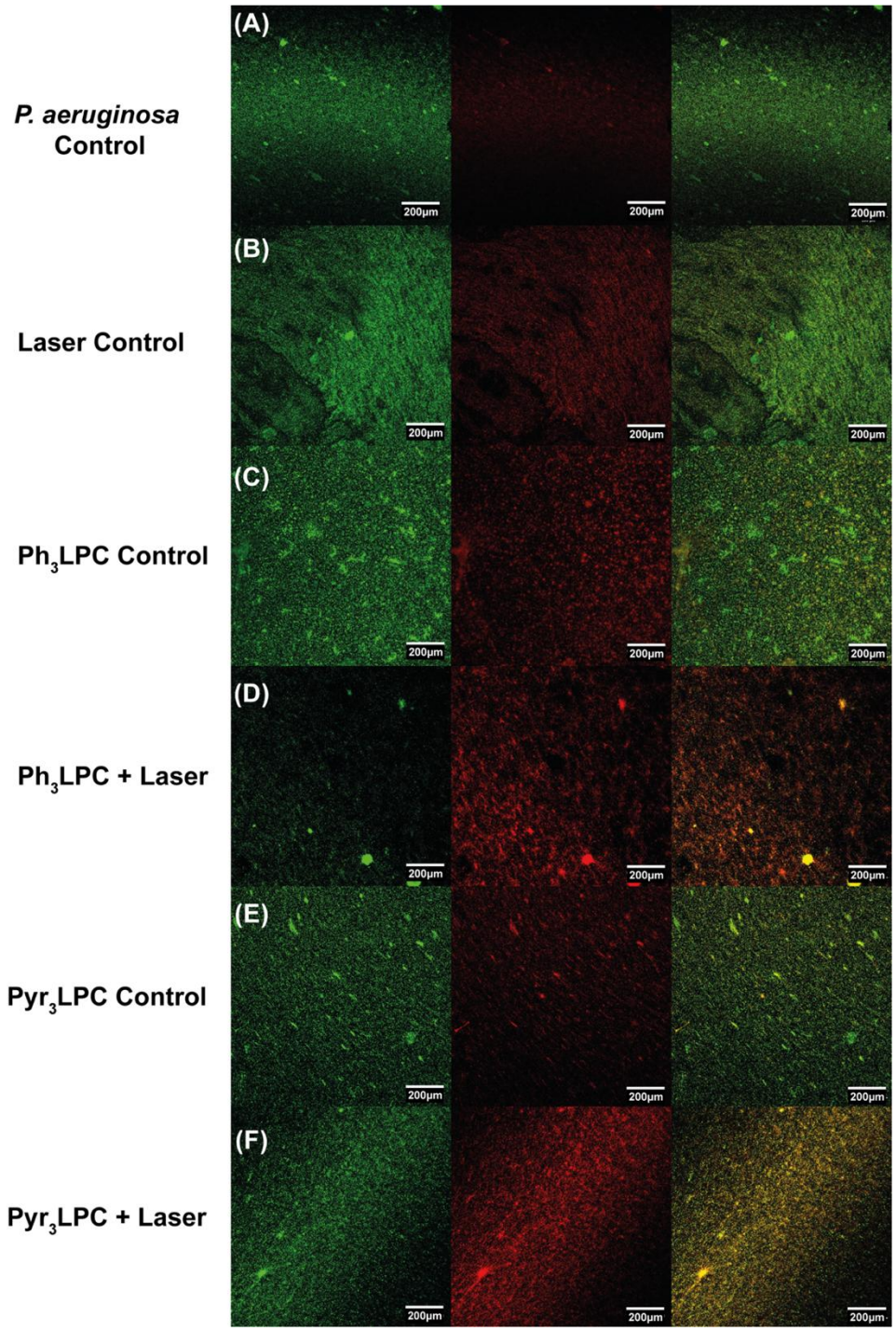

Figure 8. Confocal microscopy images of *P. aeruginosa* biofilms treated by the LIVE/DEAD™ BacLight Bacterial viability Kit. Green images correspond to alive bacteria (Syto9, left) and red ones to dead bacteria (PI, middle), while the right column is a merged image of both green and red channels. (A) *P. aeruginosa* biofilm treated with PBS (control). (B) *P. aeruginosa* biofilm after 10 min irradiation (laser control, 670 nm, 800 mW.cm^{-2}). (C) *P. aeruginosa* biofilms treated with Ph_3LPC liposomes (100 µM PS) without laser irradiation. (D) *P. aeruginosa* biofilm treated with Ph_3LPC liposomes (100 µM) with 10 min irradiation (670 nm, 800 mW.cm^{-2}). (E) *P. aeruginosa* biofilm treated with Pyr_3LPC liposomes (100 µM PS) without laser irradiation. (F) *P. aeruginosa* biofilm treated with Pyr_3LPC liposomes (100 µM PS) with 10 min irradiation (670 nm, 800 mW.cm^{-2}). The scale bar is 200 µm.

4. Conclusion

The aim of this work was to develop new nanosystems with photothermal and photodynamic properties for the treatment of bacteria and biofilm-related infections. To do so, we used newly synthesized lipid-porphyrin conjugates Ph_xLPC and Pyr_xLPC. In a previous work, we demonstrated that these conjugates were not able to form stable assemblies on their own and they needed to be incorporated at low molar concentration in a lipid matrix such as DPPC to maintain vesicle integrity. Herein, we succeeded in forming liposomes by mixing the conjugates with cholesterol at equimolar percentage and DSPE-PEG_{2000} (5% molar ratio). Interestingly, all PL-Por conjugate assemblies displayed similar absorbance and fluorescence with higher fluorescence quenching for Pyro-a conjugates. Formulations containing PL-Por with the longest linker exhibited higher stability than those with a shorter one. This could be related to deeper embedment of the porphyrin core inside the lipid matrix. Based on this result, we selected Pyr_3LPC and Ph_3LPC liposomes as the candidates for *in vitro* antimicrobial experiments. The two studied systems show almost the same photothermal effect against planktonic cultures and biofilms of *S. aureus* and *P. aeruginosa*. However, Ph_3LPC vesicles exhibit superior photodynamic activity, making them the best combination for PTT/PDT. Such results highlight the higher potential of the photodynamic activity of nanoassemblies compared to their photothermal conversion. Although very high temperatures could not be achieved with both PL-Por assemblies, this work could guide the researchers in their future works to design nanoplatforms based on other PL-Por conjugates that exhibit even higher photodynamic versus photothermal activity to eradicate efficiently the bacterial biofilms.

Acknowledgements

LGB is thankful to the French Ministry of Research for the financial support of his PhD thesis. The financial supports for Lipid-Porphyrin conjugates research from the ANR JCJC Grant (Project-ANR-19-CE09-0015) and from the Laboratory of Excellence LERMIT via an ANR grant (ANR-10-LABX-33) under the program of ‘‘Investissements d’avenir’’ are gratefully acknowledged. This project has also received financial support from the CNRS through the MITI interdisciplinary programs.

References

Aksoy, İ., Küçükkeçeci, H., Sevgi, F., Metin, Ö., Hatay Patir, I., 2020. Photothermal Antibacterial and Antibiofilm Activity of Black Phosphorus/Gold Nanocomposites against Pathogenic Bacteria. Acs Appl Mater Inter 12, 26822-26831.

Banfi, S., Caruso, E., Buccafurni, L., Battini, V., Zazzaron, S., Barbieri, P., Orlandi, V., 2006. Antibacterial activity of tetraaryl-porphyrin photosensitizers: an in vitro study on Gram negative and Gram positive bacteria. J Photochem Photobiol B 85, 28-38.

Bao, Y., Zhang, X., Jiang, Q., Xue, T., Sun, B., 2015. Pfs promotes autolysis-dependent release of eDNA and biofilm formation in Staphylococcus aureus. Medical Microbiology and Immunology 204, 215-226.

Berg, K., Selbo, P.K., Weyergang, A., Dietze, A., Prasmickaite, L., Bonsted, A., Engesaeter, B.Ø., Angell-Petersen, E., Warloe, T., Frandsen, N., HØGset, A., 2005. Porphyrin-related photosensitizers for cancer imaging and therapeutic applications. Journal of Microscopy 218, 133-147.

Bronstein, L.-G., Cressey, P., Abuillan, W., Konovalov, O., Jankowski, M., Rosilio, V., Makky, A., 2022a. Influence of the porphyrin structure and linker length on the interfacial behavior of phospholipid-porphyrin conjugates. J Colloid Interf Sci 611, 441-450.

Bronstein, L.-G., Tóth, Á., Cressey, P., Rosilio, V., Di Meo, F., Makky, A., 2022b. Phospholipid–porphyrin conjugates: deciphering the driving forces behind their supramolecular assemblies. Nanoscale.

Carter, K.A., Shao, S., Hoopes, M.I., Luo, D., Ahsan, B., Grigoryants, V.M., Song, W., Huang, H., Zhang, G., Pandey, R.K., Geng, J., Pfeifer, B.A., Scholes, C.P., Ortega, J., Karttunen, M., Lovell, J.F., 2014. Porphyrin-phospholipid liposomes permeabilized by near-infrared light. Nat Commun 5, 3546.

Charron, D.M., Yousefalizadeh, G., Buzzá, H.H., Rajora, M.A., Chen, J., Stamplecoskie, K.G., Zheng, G., 2020. Photophysics of J-Aggregating Porphyrin-Lipid Photosensitizers in Liposomes: Impact of Lipid Saturation. Langmuir 36, 5385-5393.

Chen, H., Shao, L., Ming, T., Sun, Z., Zhao, C., Yang, B., Wang, J., 2010. Understanding the Photothermal Conversion Efficiency of Gold Nanocrystals. Small 6, 2272-2280.

Costerton, J.W., Stewart, P.S., Greenberg, E.P., 1999. Bacterial biofilms: a common cause of persistent infections. Science 284, 1318-1322.
da Cunha, M.M., Trepout, S., Messaoudi, C., Wu, T.D., Ortega, R., Guerquin-Kern, J.L., Marco, S., 2016. Overview of chemical imaging methods to address biological questions. Micron 84, 23-36.
de Kraker, M.E.A., Stewardson, A.J., Harbarth, S., 2016. Will 10 Million People Die a Year due to Antimicrobial Resistance by 2050? PLOS Medicine 13, e1002184.
DeFrancesco, A.S., Masloboeva, N., Syed, A.K., DeLoughery, A., Bradshaw, N., Li, G.-W., Gilmore, M.S., Walker, S., Losick, R., 2017. Genome-wide screen for genes involved in eDNA release during biofilm formation by Staphylococcus aureus. Proceedings of the National Academy of Sciences 114, E5969-E5978.
Flemming, H.C., Wingender, J., 2010. The biofilm matrix. Nat Rev Microbiol 8, 623-633.
Hall-Stoodley, L., Costerton, J.W., Stoodley, P., 2004. Bacterial biofilms: from the natural environment to infectious diseases. Nat Rev Microbiol 2, 95-108.
Hamblin, M.R., Hasan, T., 2004. Photodynamic therapy: a new antimicrobial approach to infectious disease? Photoch Photobio Sci 3, 436-450.
Hartman, D., Perfecting Your Spread Plate Technique. Journal of Microbiology & Biology Education 12, 204-205.
Ibelli, T., Templeton, S., Levi-Polyachenko, N., 2018. Progress on utilizing hyperthermia for mitigating bacterial infections. International Journal of Hyperthermia 34, 144-156.
Ikeda, A., Satake, S., Mae, T., Ueda, M., Sugikawa, K., Shigeto, H., Funabashi, H., Kuroda, A., 2017. Photodynamic Activities of Porphyrin Derivative–Cyclodextrin Complexes by Photoirradiation. ACS Medicinal Chemistry Letters 8, 555-559.
Jiang, K., Smith, D.A., Pinchuk, A., 2013. Size-Dependent Photothermal Conversion Efficiencies of Plasmonically Heated Gold Nanoparticles. The Journal of Physical Chemistry C 117, 27073-27080.
Jung, H.S., Verwilst, P., Sharma, A., Shin, J., Sessler, J.L., Kim, J.S., 2018. Organic molecule-based photothermal agents: an expanding photothermal therapy universe. Chemical Society Reviews 47, 2280-2297.
Lebeaux, D., Ghigo, J.M., Beloin, C., 2014. Biofilm-Related Infections: Bridging the Gap between Clinical Management and Fundamental Aspects of Recalcitrance toward Antibiotics. Microbiol Mol Biol R 78, 510-543.
Lovell, J.F., Jin, C.S., Huynh, E., Jin, H., Kim, C., Rubinstein, J.L., Chan, W.C., Cao, W., Wang, L.V., Zheng, G., 2011. Porphysome nanovesicles generated by porphyrin bilayers for use as multimodal biophotonic contrast agents. Nat Mater 10, 324-332.
Mah, T.F., O'Toole, G.A., 2001. Mechanisms of biofilm resistance to antimicrobial agents. Trends Microbiol 9, 34-39.
Manesh, A., Varghese, G.M., 2021. Rising antimicrobial resistance: an evolving epidemic in a pandemic. The Lancet Microbe 2, e419-e420.
Massiot, J., Abuillan, W., Konovalov, O., Makky, A., 2022. Photo-triggerable liposomes based on lipid-porphyrin conjugate and cholesterol combination: Formulation and mechanistic study on monolayers and bilayers. Biochimica et Biophysica Acta (BBA) - Biomembranes 1864, 183812.
Massiot, J., Rosilio, V., Ibrahim, N., Yamamoto, A., Nicolas, V., Konovalov, O., Tanaka, M., Makky, A., 2018. Newly Synthesized Lipid–Porphyrin Conjugates: Evaluation of Their Self-Assembling Properties, Their Miscibility with Phospholipids and Their Photodynamic Activity In Vitro. Chemistry – A European Journal 24, 19179-19194.

Massiot, J., Rosilio, V., Makky, A., 2019. Photo-triggerable liposomal drug delivery systems: from simple porphyrin insertion in the lipid bilayer towards supramolecular assemblies of lipid–porphyrin conjugates. Journal of Materials Chemistry B 7, 1805-1823.
Pattani, V.P., Tunnell, J.W., 2012. Nanoparticle-mediated photothermal therapy: a comparative study of heating for different particle types. Lasers Surg Med 44, 675-684.
Qayyum, S., Khan, A.U., 2016. Nanoparticles vs. biofilms: a battle against another paradigm of antibiotic resistance. MedChemComm 7, 1479-1498.
Reygaert, W.C., 2018. An overview of the antimicrobial resistance mechanisms of bacteria. AIMS Microbiol 4, 482-501.
Richardson, H.H., Carlson, M.T., Tandler, P.J., Hernandez, P., Govorov, A.O., 2009. Experimental and Theoretical Studies of Light-to-Heat Conversion and Collective Heating Effects in Metal Nanoparticle Solutions. Nano Letters 9, 1139-1146.
Roper, D.K., Ahn, W., Hoepfner, M., 2007. Microscale Heat Transfer Transduced by Surface Plasmon Resonant Gold Nanoparticles. The Journal of Physical Chemistry C 111, 3636-3641.
Rosenberg, M., Azevedo, N.F., Ivask, A., 2019. Propidium iodide staining underestimates viability of adherent bacterial cells. Sci Rep-Uk 9, 6483.
Seviour, T., Winnerdy, F.R., Wong, L.L., Shi, X., Mugunthan, S., Foo, Y.H., Castaing, R., Adav, S.S., Subramoni, S., Kohli, G.S., Shewan, H.M., Stokes, J.R., Rice, S.A., Phan, A.T., Kjelleberg, S., 2021. The biofilm matrix scaffold of Pseudomonas aeruginosa contains G-quadruplex extracellular DNA structures. npj Biofilms and Microbiomes 7, 27.
Shakiba, M., Ng, K.K., Huynh, E., Chan, H., Charron, D.M., Chen, J., Muhanna, N., Foster, F.S., Wilson, B.C., Zheng, G., 2016. Stable J-aggregation enabled dual photoacoustic and fluorescence nanoparticles for intraoperative cancer imaging. Nanoscale 8, 12618-12625.
Sharman, W.M., Allen, C.M., van Lier, J.E., 2000. Role of activated oxygen species in photodynamic therapy, Methods in Enzymology. Academic Press, pp. 376-400.
Stewart, P.S., 2002. Mechanisms of antibiotic resistance in bacterial biofilms. Int J Med Microbiol 292, 107-113.
Street, C.N., Gibbs, A., Pedigo, L., Andersen, D., Loebel, N.G., 2009. In Vitro Photodynamic Eradication of Pseudomonas aeruginosa in Planktonic and Biofilm Culture. Photochemistry and Photobiology 85, 137-143.
Sugimoto, S., Sato, F., Miyakawa, R., Chiba, A., Onodera, S., Hori, S., Mizunoe, Y., 2018. Broad impact of extracellular DNA on biofilm formation by clinically isolated Methicillin-resistant and -sensitive strains of Staphylococcus aureus. Sci Rep-Uk 8, 2254.
Sun, W., Weingarten, R.A., Xu, M., Southall, N., Dai, S., Shinn, P., Sanderson, P.E., Williamson, P.R., Frank, K.M., Zheng, W., 2016. Rapid antimicrobial susceptibility test for identification of new therapeutics and drug combinations against multidrug-resistant bacteria. Emerg Microbes Infect 5, e116.
Wang, X.-L., Zeng, Y., Zheng, Y.-Z., Chen, J.-F., Tao, X., Wang, L.-X., Teng, Y., 2011. Rose Bengal-Grafted Biodegradable Microcapsules: Singlet-Oxygen Generation and Cancer-Cell Incapacitation. Chemistry – A European Journal 17, 11223-11229.
Wei, Q., Ma, L.Z., 2013. Biofilm Matrix and Its Regulation in Pseudomonas aeruginosa. Int J Mol Sci 14, 20983-21005.
WHO, 2019. Report calls for urgent action to avert antimicrobial resistance crisis
Zhang, H., 2017. Thin-Film Hydration Followed by Extrusion Method for Liposome Preparation. Methods Mol Biol 1522, 17-22.
Zmerli, I., Ibrahim, N., Cressey, P., Denis, S., Makky, A., 2021a. Design and Synthesis of New PEGylated Polydopamine-Based Nanoconstructs Bearing ROS-Responsive Linkers and a

Photosensitizer for Bimodal Photothermal and Photodynamic Therapies against Cancer. Mol Pharmaceut 18, 3623-3637.
Zmerli, I., Michel, J.-P., Makky, A., 2021b. Multifunctional polydopamine-based nanoparticles: synthesis, physico-chemical properties and applications for bimodal photothermal/photodynamic therapy of cancer. Multifunctional Materials 4, 022001.